ISSN 1063-7834, Physics of the Solid State, 2010, Vol. 52, No. 4, pp. 826–837. © Pleiades Publishing, Ltd., 2010.
Original Russian Text © G.A. Bukhtiyarova, O.N. Mart'yanov, S.S. Yakushkin, M.A. Shuvaeva, O.A. Bayukov, 2010, published in Fizika Tverdogo Tela, 2010, Vol. 52, No. 4, pp. 771–781.

LOW-DIMENSIONAL SYSTEMS AND SURFACE PHYSICS

State of Iron in Nanoparticles Prepared by Impregnation of Silica Gel and Aluminum Oxide with $FeSO_4$ Solutions

G. A. Bukhtiyarova[a], O. N. Mart'yanov[a], S. S. Yakushkin[a], M. A. Shuvaeva[a], and O. A. Bayukov[b]

[a] *Boreskov Institute of Catalysis, Siberian Branch, Russian Academy of Sciences, pr. Akademika Lavrent'eva 5, Novosibirsk, 630090 Russia*

[b] *Kirensky Institute of Physics, Siberian Branch, Russian Academy of Sciences, Akademgorodok 50, Krasnoyarsk, 660036 Russia*

e-mail: helg@iph.krasn.ru

Received July 16, 2009

Abstract—The state of iron in nanoparticles prepared by impregnating silica gel and aluminum oxide with iron(II) sulfate solutions has been investigated using Mössbauer spectroscopy. It has been revealed that the state of iron depends on the nature of the support. Iron(III) hydroxysulfate and iron(III) oxysulfate nanoparticles are formed on the surface of silica gel, and iron oxide nanoparticles are formed on the surface of aluminum oxide. An increase in the concentration of iron ions or in the size of iron-containing particles leads to hydration of the nanoparticle surface. The calcination of the samples results in the formation of ε-Fe_2O_3 oxide in a strongly disordered or amorphous state in iron-containing particles on the surface of silica gel.

DOI: 10.1134/S1063783410040268

1. INTRODUCTION

Iron-containing nanoparticles have attracted particular interest of researchers owing to the large number of existing and potentially possible practical applications. Iron oxides deposited onto silica gel or aluminum oxide are catalysts of reactions of selective oxidation of hydrogen sulfide, dehydration of ethylbenzene into styrene, conversion of water vapor, etc. From the viewpoint of possible catalytic applications, catalysts containing a nanosized active phase hold much promise. In this case, the state of iron in the system depends not only on the nature of the precursor of the active component but also on the type of the support, which substantially affects the size and structure of iron-containing particles.

In the study of the structure of nanoparticles, traditional methods of structural analysis provide a small amount of information. In this situation, Mössbauer spectroscopy, which makes it possible to identify the state and properties of the local environment of iron, turns out to be most promising.

In this work, we investigate the state of iron in catalyst samples prepared by impregnating silica gel (FS) and aluminum oxide (FA) with iron(II) sulfate solutions and subsequent heat treatment.

2. SAMPLE PREPARATION AND EXPERIMENTAL TECHNIQUE

Samples were prepared using a KSKG silica gel (OOO KhromAnalit; specific surface area, 287 m^2/g; average pore diameter, 141 Å; pore volume 0.35 cm^3/g) and granulated aluminum oxide (ZAO Industrial Catalysts; specific surface area, 224 m^2/g; average pore diameter, 122 Å; pore volume 0.73 cm^3/g). The support samples with a grain size of 0.25–0.50 mm were impregnated to water capacity with solutions of iron(II) sulfate heptahydrate (ACS, 99 + %; CAS 7782-63-0), followed by drying in air at a temperature of 110°C.

Then, the samples were calcined at different temperatures (400, 500, 600, 700, 900°C) in a muffle furnace for 4 h. The samples were prepared using solutions with three different iron concentrations: 0.015, 0.081, and 0.203 g/ml in terms of anhydrous iron sulfate $FeSO_4$. In order to enrich the samples with the ^{57}Fe isotope, approximately identical amounts of iron(II) sulfate (~0.09 g/ml) prepared from a ^{57}Fe metal plate were added to each sample. The iron contents in the samples are listed in Table 1.

The Mössbauer investigations were performed at room temperature with the use of a $^{57}Co(Cr)$ source and powdered absorbers 0.5 mm thick. The isomer chemical shifts were measured with respect to metallic iron α-Fe.

The Mössbauer spectra represented either quadrupole doublets or their superpositions with Zeeman sextets depending on the heat treatment temperature. The spectra were identified in two stages. At the first stage, the probability distributions of quadrupole splittings $P(QS)$ and hyperfine magnetic fields $P(H)$ were

Table 1. Iron concentrations in the $FeSO_4/SiO_2$ and $FeSO_4/Al_2O_3$ samples

Sample	$T = 500°C$		$T = 600°C$		$T = 700°C$		$T = 900°C$	
	Fe, %	SO_4^{2-}, %	Fe, %	SO_4^{2-}, %	Fe, %	SO_4^{2-}, %	Fe, %	SO_4^{2-}, %
0.5FS			0.69	0.36				
3FS			3.37	0.78	3.43	0.69	3.51	0.72
6FS			7.42	2.19				
0.5FA	0.37	0.66						
3FA	2.63	3.99			2.65	3.27		
6FA	5.06	7.2						

determined from the experimental spectra. The probability distributions were determined using, if required, either one group of Fe^{3+} doublets, or two groups of Fe^{3+} and Fe^{2+} doublets, or a group of Fe^{3+} doublets and a group of Fe^{3+} sextets as the initial groups of subspectra. The general chemical shifts were fitted for each group of subspectra. The specific features revealed in the distributions $P(QS)$ and $P(H)$ indicate possible nonequivalent positions or states of iron in the materials under investigation. The data obtained were used to determine the number and approximate parameters of the nonequivalent positions and to construct the model spectra. At the second stage, the model spectrum was fitted to the experimental spectrum by varying the entire set of the hyperfine structure parameters.

3. SILICA GEL

3.1. Experimental Results

Figure 1a shows the Mössbauer spectra of the initial samples (with different iron contents) prepared by

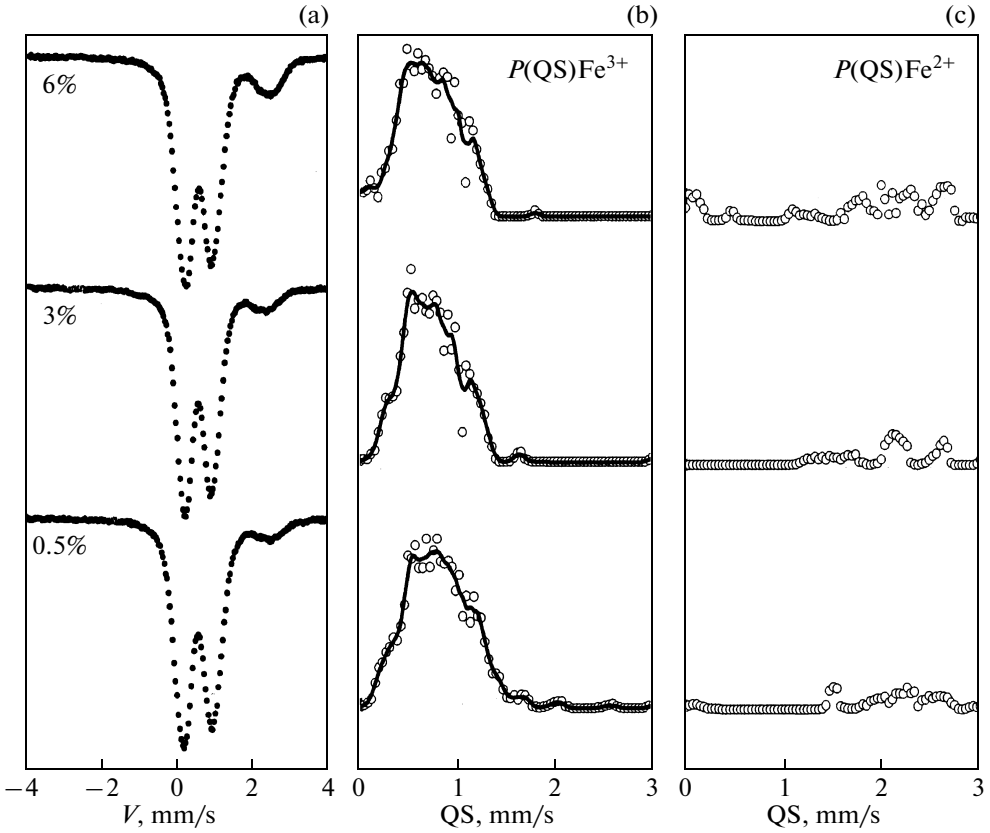

Fig. 1. (a) Mössbauer spectra of the samples prepared by impregnating the silica gel with aqueous solutions of iron sulfate at different concentrations of Fe(II) ions and (b, c) probability distributions of quadrupole splittings for (b) Fe^{3+} and (c) Fe^{2+} cations.

Table 2. Mössbauer parameters of the spectra of the samples prepared by impregnating the silica gel with $FeSO_4$ aqueous solutions at different concentrations

Sample	IS ±0.005 mm/s	QS ±0.02 mm/s	*W* ±0.02 mm/s	*A* ±0.03	Position
0.5FS	0.418	0.51	0.36	0.34	Fe1—$Fe_2O(SO_4)_2$
	0.422	0.82	0.30	0.27	Fe2—$FeOHSO_4 \cdot 2H_2O$
	0.429	1.16	0.37	0.29	Fe3—$FeOHSO_4$
	1.096	1.88	0.28	0.02	Fe^{2+} in Fe1
	1.309	2.20	0.56	0.09	Fe^{2+} in Fe2
3FS	0.419	0.49	0.33	0.38	Fe1—$Fe_2O(SO_4)_2$
	0.426	0.80	0.31	0.34	Fe2—$FeOHSO_4 \cdot 2H_2O$
	0.420	1.13	0.30	0.17	Fe3—$FeOHSO_4$
	1.157	1.61	0.36	0.04	Fe^2 in Fe1
	1.187	2.15	0.37	0.06	Fe^{2+} in Fe2
	1.245	2.59	0.23	0.02	Fe^{2+} in Fe3
6FS	0.420	0.51	0.34	0.34	Fe1—$Fe_2O(SO_4)_2$
	0.421	0.86	0.33	0.31	Fe2—$FeOHSO_4 \cdot 2H_2O$
	0.428	1.21	0.31	0.14	Fe3—$FeOHSO_4$
	1.255	1.68	0.48	0.09	Fe^{2+} in Fe1
	1.292	2.29	0.46	0.11	Fe^{2+} in Fe2

impregnating the silica gel with the aqueous solutions of the iron(II) sulfate. The probability distributions of quadrupole splittings for the positions occupied by Fe^{3+} and Fe^{2+} cations are presented in Figs. 1b and 1c, respectively. The specific features and maxima in the probability distribution curves indicate that the samples contain several nonequivalent positions of these cations. The results of the two-stage identification of the spectra are summarized in Table 2. The isomer chemical shift (IS) characterizes the electron density at the iron nucleus, the formal valence, the coordination with respect to ligands, and the degree of covalence of bonds. The quadrupole splitting (QS) characterizes the degree of deviation of the local symmetry of the electric field at the nucleus from a cubic symmetry. The absorption line width *W* (as compared to a natural width of 0.24 mm/s) characterizes the scatter of the hyperfine structure parameters (IS, QS) for positions of a particular type in the material, and the area under the partial spectrum *A* characterizes the relative occupancy of this position in the sample by iron.

The results obtained suggest that the system exhibits several nonequivalent states of iron, which indicates that the material has a multiphase composition and/or is crystallographically inhomogeneous. Chemical shifts of 0.42–0.43 mm/s are characteristic of high-spin Fe^{3+} cations, which have an octahedral coordination with respect to oxygen with a high degree of covalence of the iron–oxygen bond.

Chemical shifts of 1.0–1.3 mm/s are inherent in Fe^{2+} cations. Therefore, the initial samples that were prepared by impregnating the silica gel with the iron(II) sulfate solution and dried at a temperature of 110°C contain iron predominantly in the trivalent state. The fraction of iron in the divalent state is insignificant.

3.2. Identification of Positions

Mössbauer spectroscopy provides information on the properties of the local environment of the iron ion, whereas the question as to the phase state of the material under investigation remains open. The local environment can be identified by comparing its parameters with the parameters for the local environment in materials with the known crystal structure. In our case, it is reasonable to analyze the known Mössbauer parameters of sulfates, hydrosulfates, oxosulfates, and hydrates. The Mössbauer parameters of some sulfates are presented in Table 3.

For trivalent iron sulfates, the Mössbauer parameters for different local states differ insignificantly. Most likely, the electron shell of the Fe^{3+} ions rather objectively reflects the symmetry of the environment. For divalent iron sulfates with different degrees of hydration, the correlation between the local state and Mössbauer parameters is absent. It seems likely that this is associated with the larger valence contribution of the sixth electron in the shell of the Fe^{2+} ion, as a result of which the nuclei have a lower "sensitivity" to the lattice contribution to the electric field gradient at the nucleus.

Table 3. Mössbauer parameters of the spectra of some sulfates

	Sulfate	IS, mm/s	QS, mm/s	References
Fe^{3+}	$Fe_2(SO_4)_3$	0.47–0.50	0	[1]
	$Fe_2(SO_4)_3 \cdot 3H_2O$	0.50–0.55	0.38	[1]
	$Fe_2O(SO_4)_2$	0.37–0.57	0	[1–3]
	$Fe_2O(SO_4)_2 \cdot xH_2O$	0.41–0.43	0.4–0.69	[2]
	$FeOHSO_4$	0.42–0.48	1.25–1.45	[2–4]
	$FeOHSO_4 \cdot 2H_2O$	0.44	0.97	[4]
	$Fe_2O_2SO_4$	0.25	0.80	[3]
Fe^{2+}	$FeSO_4$	1.15–1.47	2.78–2.90	[1]
	$FeSO_4 \cdot H_2O$	1.22–1.25	2.78–2.94	[1]
	$FeSO_4 \cdot 3H_2O$	1.18	2.88	[1]
	$FeSO_4 \cdot xH_2O$ ($x = 4$–7)	1.27–1.35	2.67–3.27	[2]
	$FeSO_4 \cdot 7H_2O$	1.21–1.25	2.88–3.20	[1]

A comparison of the parameters of the spectra observed for catalysts of the FS series (Table 2) with the parameters for different iron sulfates (Table 3) allows us to identify the revealed iron positions in the system prepared by impregnating the silica gel with the $FeSO_4$ solution.

In the system, there are three positions of trivalent iron, i.e., Fe1, Fe2, and Fe3, and three positions of divalent iron. In the initial samples, the occupancies of all three positions of Fe^{3+} ions are close to each other. The Fe1, Fe2, and Fe3 positions can be identified with oxysulfate ($Fe_2O(SO_4)_2$), hydroxysulfate hydrate ($FeOHSO_4 \cdot 2H_2O$), and hydroxysulfate ($FeOHSO_4$) of trivalent iron, respectively. It should be emphasized that the assignment of the positions to a particular compound does not mean the presence of the phase but only reflects the similarity of the electronic state of iron in these positions to the electronic state in the aforementioned bulk materials.

In these samples, iron in the divalent state amounts to a small fraction as compared to trivalent iron. The quadrupole splitting for iron ions in the corresponding positions is considerably smaller than those for the known iron(II) sulfates. This suggests that these positions belong to the structure of iron(III) sulfates and arise as a result of the deficit of the negative charge of anions in the local environment. The Fe^{2+} cations predominantly occupy the Fe1 and Fe2 positions. An increase in the concentration of the $FeSO_4$ solution and the fraction of larger particles leads to an increase in the Fe^{2+} content. We can assume that the Fe1 and Fe2 positions are occupied by the ions contained in the bulk, whereas the Fe3 positions are occupied by the ions located on the surface.

4. ALUMINUM OXIDE

4.1. Experimental Results

Figure 2a shows the Mössbauer spectra of the initial samples (FA) prepared by impregnating aluminum oxide with the aqueous solutions with different concentrations of iron ions: 0.015, 0.081, and 0.203 g/ml in terms of the anhydrous iron sulfate $FeSO_4$. The probability distributions of quadrupole splittings for the positions occupied by Fe^{3+} cations are presented in Fig. 1b. The specific features in the probability distribution of quadrupole splittings indicate that the samples contain several nonequivalent iron positions. The results of the two-stage identification of the spectra are given in Table 4.

In the system, there are three iron positions that differ in the degree of distortion of the local environment. The isomer chemical shifts are characteristic of Fe^{3+} cations that have an octahedral coordination with respect to oxygen. An increase in the iron concentration leads to a noticeable increase in the chemical shifts. The modeling of the experimental spectrum of the 0.5FA sample requires the introduction of the singlet with a very large line width and a small chemical shift.

4.2. Identification of Positions

The isomer chemical shifts observed for the FA samples are typical of a number of oxide and hydroxide compounds of iron. The Mössbauer parameters of these compounds are listed in Table 5. It can be seen from this table that the isomer chemical shift somewhat increases upon changing over from iron oxides to iron hydroxides, namely, from 0.33 mm/s for α-Fe_2O_3 to 0.40 mm/s for ferrihydrite of the bacterial origin (Table 5). With a decrease in the size of oxide and hydroxide particles and their transition to the super-

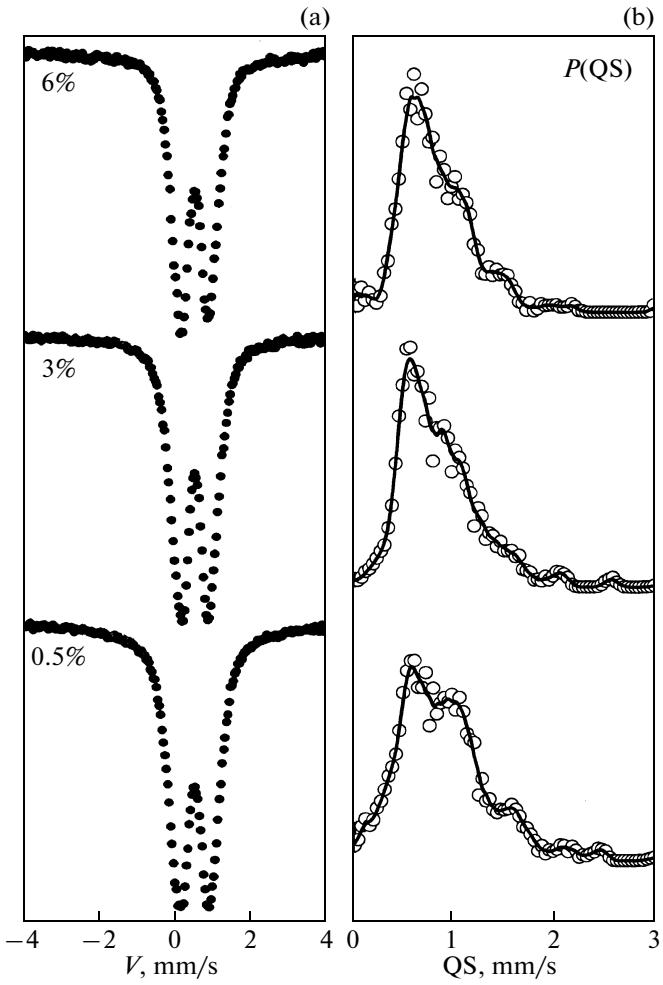

Fig. 2. (a) Mössbauer spectra of the samples prepared by impregnating the aluminum oxide with $FeSO_4$ aqueous solutions at different concentrations of Fe(II) ions and (b) probability distributions of quadrupole splittings for Fe^{3+} cations.

paramagnetic state (SPM), additional positions with a larger quadrupole splitting as compared to those for massive materials manifest themselves in the spectra. Different viewpoints regarding the appearance of distorted positions are available in the literature. In [5, 12, 13], the distorted positions are assigned to surface cations. In [9–11], two types of positions are attributed to different configurations of ligands of two types in the coordination polyhedron (oxygen and hydroxyl group). Vandenberghe et al. [12] believe that two positions are associated with the ferrihydrite regions with different degrees of crystallinity: regions $6L$ with a high degree of crystallinity are characterized by six X-ray diffraction lines, and regions $2L$ exhibit an X-ray diffraction pattern with two lines.

The structure of the ferrihydrite of the bacterial origin with the chemical composition corresponding to the formula $Fe_5HO_8 \cdot 4H_2O$ involves up to four nonequivalent iron positions [17, 18]. In this case, the chemical shift is larger than the chemical shifts for the known hydroxides, probably, due to the excess of crystal water. Reasoning from the neutron diffraction [19] and Mössbauer data [17, 18], it was assumed that the appearance of nonequivalent positions in poorly crystallized ferrihydrites is associated with different packings of ligand layers. In the case of a close cubic packing, the sequence of ligand layers is represented as *ABCABC*.... For this packing, the octahedral and tetrahedral positions are formed in the structure and the neighboring coordination octahedra are shared by edges. The local symmetry of edge-shared octahedra is rather high. These positions in Table 4 are designated as Fe1. The corresponding positions occur in spinels and double iron layers in ferrihydrite.

The close hexagonal packing of ligands leads to the sequence *ABAB*..., and coordination octahedra are shared by faces. In this case, the iron cations of the neighboring octahedra appear to be at the shortest distance from each other; as a result, they are repelled from each other, thus decreasing the local symmetry. In our work, these positions are designated as Fe2. They are formed in the lattice of hematite α-Fe_2O_3 and single iron layers in ferrihydrite. In poorly crystallized ferrihydrite nanoparticles, a strict sequence of ligand layers is disturbed and the ligand sublattice represents a set of random sequences of oxygen atoms and hydroxyl groups with elements of hexagonal and cubic packings. The occupancies of the Fe1 and Fe2 positions depend on the ratio between the formed packings of ligand layers. The idealized ferrihydrite structure is characterized by the layer sequence *ABACACABACAC*... providing an occupancy ratio of 2 : 1 between the Fe1 and Fe2 positions, which is observed for sufficiently well-crystallized ferrihydrites.

5. DISCUSSION OF THE RESULTS

The structure of the initial samples of catalysts of the FA series contains three nonequivalent iron positions (Table 4). The Fe1 positions can be assigned to iron ions with a predominantly cubic packing of ligand layers, and the Fe2 positions can be attributed to regions with the hexagonal packing. The Fe3 positions can correspond to interblock or surface iron. When the aluminum oxide is impregnated with the aqueous solution at the low concentration of iron ions (0.5 wt %), the chemical shift (0.35 mm/s) characterizes Fe^{3+} cations in the oxygen environment. The dominant occupation of the Fe2 position indicates that the hexagonal packing of oxygen ions predominantly occurs in the material. It seems likely that the hexagonal crystal structure of the substrate (aluminum oxide) favors the formation of the close hexagonal packing of oxygen in the thin layer of the deposited iron compound. We can assume that the regularity and small lattice constant of the substrate are responsible for the displacement of sulfate ions from the precipitate.

Table 4. Mössbauer parameters of the spectra of the samples prepared by impregnating the aluminum oxide with $FeSO_4$ aqueous solutions at different concentrations

Sample	IS ±0.005 mm/s	QS ±0.02 mm/s	W ±0.02 mm/s	A ±0.03	Position
0.5FA	0.359	0.56	0.34	0.25	Fe1 (cubic)
	0.349	0.97	0.50	0.56	Fe2 (hexagonal)
	0.346	1.54	0.28	0.03	Fe3 (interblock)
	0.190	0	1.46	0.16	Relaxation spectrum
3FA	0.369	0.57	0.33	0.39	Fe1 (cubic)
	0.365	0.93	0.45	0.52	Fe2 (hexagonal)
	0.396	1.41	0.43	0.09	Fe3 (interblock)
6FA	0.374	0.57	0.37	0.41	Fe1 (cubic)
	0.382	0.84	0.41	0.42	Fe2 (hexagonal)
	0.410	1.23	0.39	0.16	Fe3 (interblock)

Table 5. Mössbauer parameters of the spectra of some iron oxides and iron hydroxides

Compound	IS, mm/s	QS, mm/s	Position	References
SPM α-Fe_2O_3	0.30–0.33	0.52	Bulk	[5]
		0.80–0.92	Surface	
SPM β-Fe_2O_3	0.36	0.69		[6–8]
	0.37	0.90		
β-FeOOH	0.36–0.38	0.51–0.56	$O_2(OH)_4$	[9–11]
	0.38	0.92–0.96	$O_3(OH)_3$	
γ-FeOOH	0.36–0.37	0.54–0.7	Bulk	[12, 13]
		1.10	Surface	
$Fe_5HO_8 \cdot 4H_2O$	0.36–0.38	0.60	6*L*	[12, 14]
	0.37–0.38	0.96	2*L*	
	0.34–0.36	0.54–0.57		[15, 16]
	0.34–0.35	0.87–1.00		
	0.38–0.40	0.52–0.59	Fe1 (cubic)	[17, 18]
	0.38–0.41	0.89–1.06	Fe2 (hexagonal)	
	0.39–0.40	1.31–1.53	Fe3 (interblock)	
	0.39–0.40	1.80–1.85	Fe4 (surface)	

An increase in the concentration of iron ions results in an increase in the chemical shift for all positions in the FA samples; in this case, the largest increase is observed for the Fe3 positions. This is associated with the fact that an increase in the particle size leads to a decrease in the influence of the substrate and to the hydration of the material. A considerable increase in the chemical shift for the Fe3 positions indicates that water is predominantly bonded to interblock iron. The question as to whether this water is crystal water or is represented by hydroxyl groups remains open. An increase in the concentration of iron ions results in an increase in the occupancy of iron positions associated with the cubic packing of ligands, which also reflects a decrease in the influence of the substrate with an increase in the size of iron-containing particles. An increase in the occupancy of the interblock iron positions Fe3 is most likely explained by the equalization of the occupancies of the regions in the material with the cubic and hexagonal packings of ligands when the size of the interface between the regions becomes maximum.

The singlet with the very large width of the absorption line is separated in the spectrum of the 0.5FA sample. It seems likely that this singlet represents an unresolved relaxation sextet associated with the single

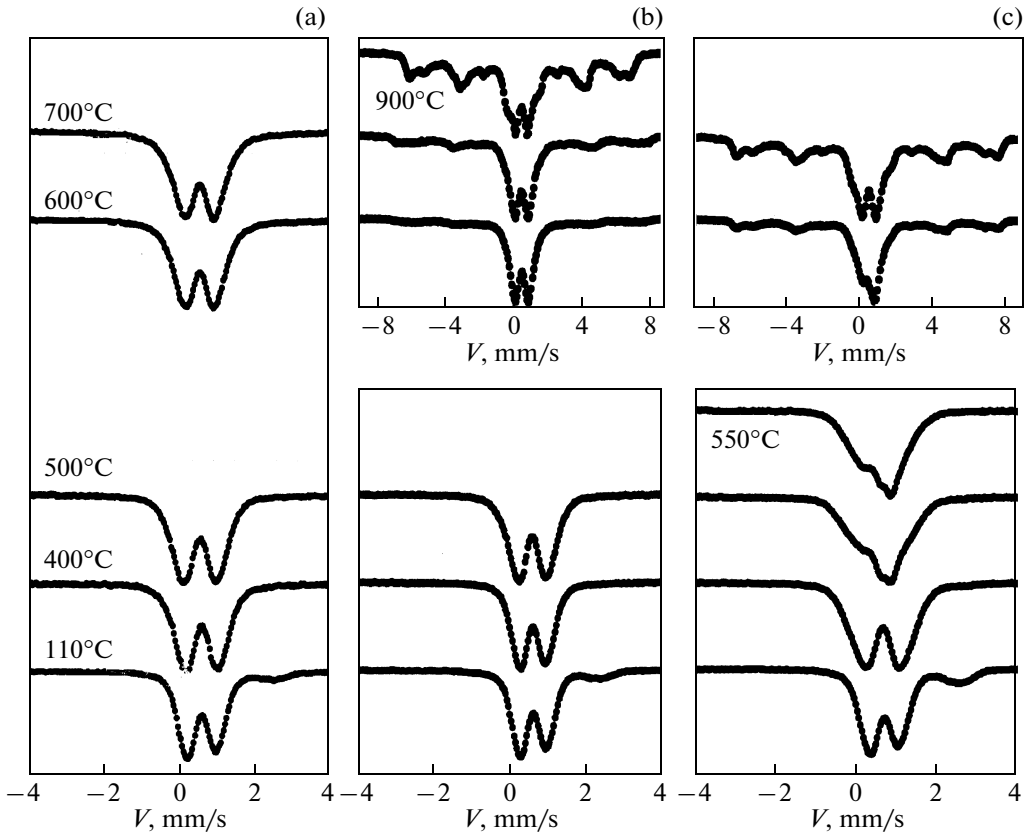

Fig. 3. Mössbauer spectra of the (a) 0.5FS, (b) 3FS, and (c) 6FS samples after calcination of the initial samples at different temperatures in air.

iron atoms that are embedded in the bulk of the aluminum oxide and undergo slow relaxation [20].

The impregnation of the silica gel with the $FeSO_4$ aqueous solution and subsequent drying at a temperature of 110°C in air results in the formation of iron-containing nanoparticles, in which iron ions are predominantly in the trivalent state and occupy octahedral positions. Large isomer chemical shifts as compared to those for iron oxide compounds suggest that iron is bonded to SO_4^{2-} ligands. The system contains three nonequivalent positions of iron ions, for which the local environment is similar to the environment in the oxysulfate $Fe_2O(SO_4)_2$, hydroxysulfate $FeOHSO_4$, and hydroxysulfate dihydrate $FeOHSO_4 \cdot 2H_2O$. Judging from the Mössbauer parameters, a small amount of divalent iron does not enter into the composition of the $FeSO_4$ compound and is formed in the lattices of the revealed sulfates due to the local deficit of the anion charge. Probably, the amorphous structure of the silica gel does not provide the conditions for the formation of oxides but favors the formation of sulfates with large interionic distances.

6. INFLUENCE OF HEAT TREATMENT ON THE STATE OF IRON IN THE SAMPLES PREPARED BY IMPREGNATION OF SILICA GEL WITH $FeSO_4$ AQUEOUS SOLUTIONS

Figure 3 shows the Mössbauer spectra measured for the 0.5FS, 3FS, and 6FS samples at room temperature after calcination at different temperatures. The analysis of the spectral shape demonstrates that the initial samples contain a small amount of divalent iron, which increases with an increase in the concentration of deposited iron. The spectra of the 0.5FS sample exhibit quadrupole doublets, which remain almost unchanged with an increase in the heat treatment temperature to 700°C. In the spectrum of the 3FS sample after the heat treatment at temperatures higher than 500°C, there appears a Zeeman sextet with the intensity increasing with an increase in the annealing temperature. In the spectrum of the 6FS sample at an annealing temperature of 500°C, there arises a feature, which disappears at temperatures above 600°C. Most likely, this feature is associated with the metastable phase. The intensity of the sextet in the spectrum of the 6FS sample is higher than that of the 3FS sample at the corresponding temperatures, which indicates the formation of the magnetically ordered phase in the 6FS sample at earlier stages of heat treatment.

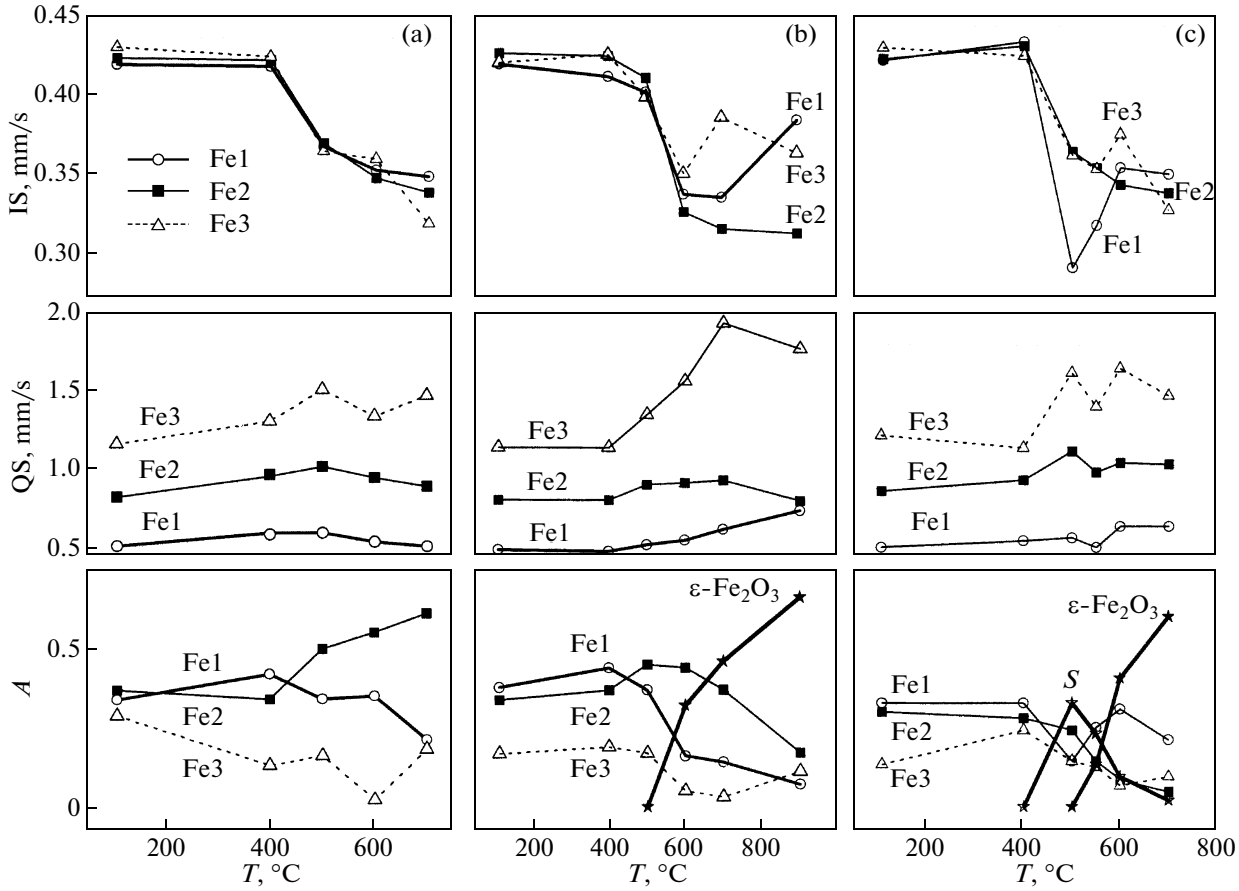

Fig. 4. Dependences of the isomer chemical shift IS, the quadrupole splitting QS, and the occupancy of nonequivalent iron positions A on the calcination temperature for the (a) 0.5FS, (b) 3FS, and (c) 6FS samples.

We performed the two-stage identification of the spectra, according to which the model spectrum was constructed using the probability distributions of quadrupole splittings for doublets and hyperfine fields for sextets. The results of the identification in the form of the dependences of the Mössbauer parameters on the annealing temperature for the main iron positions are presented in Fig. 4.

The heat treatment of the initial samples of the catalysts at temperatures lower than 400°C does not result in substantial changes in the Mössbauer spectra, except for the changes associated with the oxidation of a small amount of the impurity of divalent iron to the trivalent state. The heat treatment at a temperature of 500°C leads to a drastic decrease in the chemical shift to values characteristic of the iron oxide, which suggests the transformation of the sulfate into the iron oxide. In the 0.5FS sample (Fig. 4a), iron oxide nanoparticles with a predominantly hexagonal packing of oxygen atoms are formed up to the highest calcination temperatures, which is evidenced by an increase in the occupancy of the Fe2 positions as compared to the Fe1 positions.

In the samples with the higher iron concentration (the 3FS sample), the calcination at temperatures above 500°C is accompanied by sintering oxide particles to rather large particles of the magnetically ordered phase, as can be judged from the appearance of the sextet in the spectrum. For small particle sizes (below 500°C), thermal fluctuations of the magnetic moment of the particle become significant and particles undergo a transition to the so-called superparamagnetic state. The superparamagnetic behavior at room temperature for the majority of magnetic oxides is observed for particle sizes of smaller than 20 nm [21]. The calcination of the 3FS sample at a temperature of 500°C leads to an increase in the occupancy of the Fe2 positions (Fig. 4b), which correspond to the hexagonal packing of oxygen atoms.

At a calcination temperature of 600°C, the magnetically ordered phase is formed by the iron ions that occupy the positions with the hexagonal and cubic packings of oxygen atoms and, to a smaller extent, by interblock iron ions (Fe3 positions). The fraction of the magnetically ordered phase at a calcination temperature of 900°C amounts to 70% of the total iron content in the system.

Table 6. Mössbauer parameters of the spectra of the ε-Fe_2O_3 phase formed during the calcination of the samples prepared by impregnating the silica gel with $FeSO_4$ aqueous solutions and Néel temperatures (available in the literature) calculated for different distributions of iron cations over the positions in the ε-Fe_2O_3 phase

	IS ±0.005 mm/s	H ±5 kOe	QS ±0.02 mm/s	W_{34-16} ±0.02 mm/s	A ±0.03	Position	T_N, K
3FS 900°C	0.390	436	–0.52	0.22–0.64	0.224	*B*1	470
	0.389	388	–0.25	0.85	0.297	*B*2	
	0.347	343	0	1.04	0.124	*B*3	
	0.239	251	–0.23	1.06	0.355	*A*4	
6FS 700°C	0.394	443	–0.50	0.24–0.57	0.218	*B*1	658
	0.402	395	–0.25	0.95	0.360	*B*2	
	0.292	339	0	1.18	0.118	*B*3	
	0.220	256	–0.33	1.02	0.300	*A*4	
ε-Fe_2O_3	0.37	450	–0.19	0.24	0.239	*B*1	340
[22]	0.39	452	–0.06	0.24	0.239	*B*2	
	0.38	395	0	0.37	0.268	*B*3	
	0.21	262	–0.07	0.42	0.254	*A*4	
ε-Fe_2O_3	0.38	448	–0.05		0.194	*B*1	306
[23]	0.36	446	–0.19		0.208	*B*2	
	0.37	391	–0.02		0.351	*B*3	
	0.21	258	–0.05		0.247	*A*4	
ε-Fe_2O_3					0.25	*B*1	369
($A/B = 0.25$,					0.25	*B*2	
calculation)					0.25	*B*3	
					0.25	*A*4	
ε-Fe_2O_3					0.2	*B*1	236
($A/B = 0.4$,					0.2	*B*2	
calculation)					0.2	*B*3	
					0.4	*A*4	

During the calcination of the initial 6FS samples, there appears an additional position of iron ions (designated as *S* in Fig. 4c), which is characterized by the following Mössbauer parameters: IS = 0.54 mm/s, QS = 0.28 mm/s, and $W = 0.37$ mm/s. At a calcination temperature of 600°C, the concentration of *S* position is equal to 34%. In this case, the observed Mössbauer parameters are close to those for the sulfate hydrate $Fe_2(SO_4)_3 \cdot 3H_2O$ [1] (Table 3). An increase in the calcination temperature to 700°C results in the disappearance of the *S* position, which indicates that the corresponding iron state is metastable.

7. THE ε-Fe_2O_3 PHASE

The Mössbauer parameters of the magnetically ordered phase formed during the calcination of the silica gel samples prepared according to the incipient wetness impregnation with the aqueous solution of the iron(II) sulfate are listed in Table 6. A comparison of the parameters of the observed spectra with the data available in the literature [22, 23] allows us to make the inference that the calcination of the initial samples of the FS series at temperatures above 500°C leads to the formation of particles of the iron oxide ε-Fe_2O_3. The widths of the inner (third and fourth) and outer (first and sixth) lines of the sextet are presented in the column W_{34-16} in Table 6. One number is given if these quantities coincide with each other.

The parameters for the *A*4 tetrahedral positions are closest to the data available in the literature. The hyperfine fields at the octahedral positions for the samples under investigation are noticeably lower than those presented in [22, 23]. However, it is worth noting that the line widths of the observed sextets are large. The broadening of the outer lines of the sextet as compared to the inner lines for the *B*1 positions is caused by the scatter of the hyperfine fields at the nuclei of the Fe^{3+} ions. This effect is not observed for the *B*2 and *B*3 positions. In this case, the large line widths indicate

the scatter in the electron densities and electric field gradients. We can assume that the state of the ε-Fe_2O_3 oxide formed differs substantially from the crystalline sate described in [22, 23].

Previously, the results of the study of the crystal structure of the ε-Fe_2O_3 oxide by X-ray diffraction made it possible to determine the symmetry group [22] and to refine the atomic coordinates [24]. It was demonstrated that the structure of the ε-Fe_2O_3 oxide is based on the close packing of oxygen atoms with the alternation of layers *ABAC*.... This packing in the lattice leads to the formation of octahedral (*B*) and tetrahedral (*A*) iron positions with the ratio $A/B = 0.25$ for the disordered distribution of cations and the ratio $A/B = 0.40$ for the ordered distribution of cations.

In our materials, the ratio A/B between the occupancies differs from those corresponding to the ordered and disordered structures of the ε-Fe_2O_3 oxide, which probably indicates a strongly disordered distribution of iron cations over the crystallographic positions of the oxide or its amorphous structure. Most likely, a random set of elements of the cubic and hexagonal packings of oxygen atoms in iron nanoparticles favors the formation of a random distribution of cations. The degree of disorder affects the occupancy of the tetrahedral and octahedral positions. It should be noted that, in ferrihydrites of the bacterial origin with the structure characterized by a random sequence of the cubic and hexagonal packings of ligands, the calcination in air results in the formation of the amorphous ferrite phase [18] with the Mössbauer parameters close to those for the ε-Fe_2O_3 oxide.

Tronc et al. [22] assumed that the ε-Fe_2O_3 oxide is a noncollinear four-sublattice ferrimagnet. However, reasoning from the results of the magnetic susceptibility measurements for small-sized (130 Å) ε-Fe_2O_3 particles, Dezsi and Coey [25] made the inference that this oxide is an antiferromagnet with the Néel temperature $T_N = 480$ K. We analyzed the exchange interactions in the structure of the ε-Fe_2O_3 oxide in the framework of the indirect coupling model [26, 27], which allows us not only to calculate the exchange integrals but also to predict the magnetic structure and to estimate the Néel temperature. According to the model, the structure of the ε-Fe_2O_3 oxide can be characterized by five integrals of the cation–cation exchange interaction: three integrals that describe the interaction of the Fe^{3+} cations occupying the octahedral positions

$$J(180^\circ) = -\frac{4}{25}\left(\frac{8}{9}b^2 + c^2\right)U \quad (-11.6\ \text{K}),$$

$$J(131^\circ) = -\frac{4}{25}\left(\frac{8}{9}b^2 + c^2\right)U|\cos 131^\circ| \quad (-7.6\ \text{K}),$$

Table 7. Integrals of intersublattice exchange interactions in the structure of the ε-Fe_2O_3 oxide (in K) according to the prediction of the indirect coupling model

	1	2	3	4
1	−36.4	−52.6	−55.6	−27.7
2	−52.6	0	−54.6	−110.8
3	−55.6	−54.6	−37.6	−83.1
4	−27.7	−110.8	−83.1	−285.2

$$J(90^\circ) = -\frac{4}{75}c(8b + c)U \quad (-18.2\ \text{K});$$

the integral that describes the intersublattice (*AB*) interaction between the Fe^{3+} cations in the tetrahedral and octahedral positions

$$J(125^\circ) = -\frac{4}{75}a(2b + 3c)U \quad (-27.7\ \text{K});$$

and the integral that describes the intrasublattice interaction between the Fe^{3+} cations in the tetrahedral positions

$$J(110^\circ) = -\frac{6}{25}a^2U \quad (-285.2\ \text{K}).$$

In the above relationships, *a*, *b*, and *c* are cation–cation electron hopping parameters representing the square of the admixture coefficient in the expression for the anibonding molecular orbital. The parameter *a* characterizes the transfer in the tetrahedron geometry; the parameters *b* and *c* characterize the transfer in the octahedron geometry for the σ and π bonds, respectively; and *U* is the electronic excitation energy in the transfer from the oxygen ion to the Fe^{3+} ion. According to the data available in the literature [27], these parameters for oxide spinels are as follows: $a = 0.08$, $b = 0.02$, $c = 0.01$, and $U = 8$ eV. In the structure of the ε-Fe_2O_3 oxide, the interionic distance in the tetrahedron is close to the corresponding distance in spinels. The distance in the octahedron is considerably smaller. Taking into account a strong dependence of the transfer integral on the interionic distance, the above parameters for the structure of the ε-Fe_2O_3 oxide were taken to be $a = 0.08$, $b = 0.025$, $c = 0.015$, and $B = 8$ eV. The estimates of the exchange integrals for the oxide structure under investigation are presented in parentheses after the formulas. With allowance made for the number of the nearest neighbors, we obtained the intersublattice interactions for the ordered structure of the ε-Fe_2O_3 oxide proposed in [22] (Table 7). The crystallographic sublattices are designated according to the designations of cations in [22].

All integrals are negative; i.e., they favor the antiferromagnetic ordering. The model predicts the maximum interaction for the nearest cations in the tetrahedral environment (−285 K). This leads to the separa-

Table 8. Integrals of intersublattice exchange interactions in the structure of the ε-Fe_2O_3 oxide (in K) according to the prediction of the indirect coupling model for the case of eight magnetic sublattices

	1↑	1↓	2↑	2↓	3↑	3↓	4↑	4↓
1↑	0	−36.4	−26.8	−25.8	−29.8	−25.8	0	−27.7
1↓	−36.4	0	−25.8	−26.8	−25.8	−29.8	−27.7	0
2↑	−26.8	−25.8	0	0	−18.2	−36.4	−55.4	−55.4
2↓	−25.8	−26.8	0	0	−36.4	−18.2	−55.4	−55.4
3↑	−29.8	−25.8	−18.2	−36.4	0	−36.4	−27.7	−55.4
3↓	−25.8	−29.8	−36.4	−18.2	−36.4	0	−55.4	−27.7
4↑	0	−27.7	−55.4	−55.4	−27.7	−55.4	0	−285.2
4↓	−27.7	0	−55.4	−55.4	−55.4	−27.7	−285.2	0

tion of cations in the tetrahedral coordination into two antiferromagnetic sublattice, which results in the separation of octahedral cations into additional sublattices. Therefore, four crystallographic sublattices are divided into eight magnetic sublattices. The calculated exchange integrals for this model are listed in Table 8.

The analysis of the ratio between the exchange integrals in this system allows us to determine the mutual orientation of the sublattice magnetic moments (shown in the table by arrows near the numbers of the sublattices). The magnetic structure predicted by the indirect coupling model for the ε-Fe_2O_3 oxide (the mutual orientation of magnetic moments) is shown by arrows on the numbers of crystallographic positions in Fig. 5. The Néel temperature for this system $T_N = 369$ K differs significantly from the experimental Néel temperature $T_N = 480$ K [25].

The data presented in Tables 6 and 7 were obtained for the ordered structure of the ε-Fe_2O_3 oxide, i.e., for the ratio $A/B = 0.25$. Tronc et al. [22] considered the disordered distribution of cations over the crystallographic positions in the structure of the ε-Fe_2O_3 oxide, for which the ratio between the position occupancies is $A/B = 0.4$. Since the B positions have identical occupancies, the indirect coupling model predicts the Néel temperature $T_N = 236$ K. Therefore, the Néel temperature depends substantially on the cation distribution. In the structure, where the number of vacant positions is larger than the number of entering iron cations, cations can be randomly distributed over positions, which leads to the observed dependence. The Mössbauer spectroscopy makes it possible to determine the occupancies of nonequivalent positions in materials, i.e., to reveal the formed cation distribution. These distributions for the ε-Fe_2O_3 oxides according to the data available in the literature [22, 23] and for the ε-Fe_2O_3 phase identified in the samples prepared by impregnating the silica gel with the iron sulfate solution are presented in the column A in Table 6. The Néel temperatures estimated for these cation distributions are given in the last column in Table 6. It can be seen from this table that the Néel temperature of the ε-Fe_2O_3 oxide can depend significantly on the oxide synthesis condition.

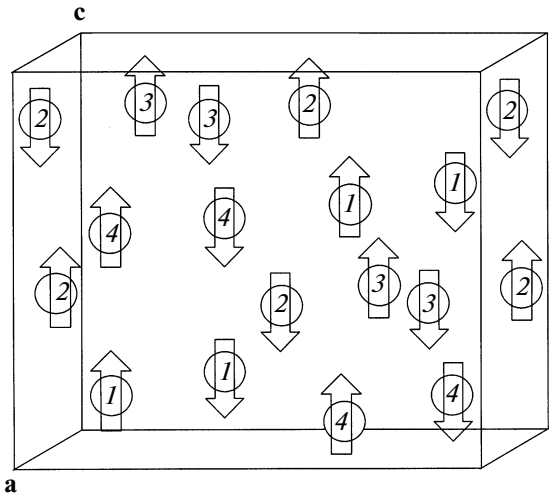

Fig. 5. Magnetic structure of the ε-Fe_2O_3 oxide. Only iron cations are shown. Arrows on the numbers of the sublattices indicate the mutual direction of the magnetic moments of the cations.

Therefore, the ε-Fe_2O_3 oxide formed in the system under consideration represents an eight-sublattice antiferromagnet. Small-sized ε-Fe_2O_3 oxide particles can have nonzero net magnetic moment due to the "parasitic" moment arising on the crystallite surface or the canting of the moments of the magnetic sublattices.

8. CONCLUSIONS

Thus, by summarizing the data obtained in our work, the conclusion can be drawn that iron(III) hydroxysulfate and iron(III) oxysulfate nanoparticles are formed in the samples prepared by the incipient wetness impregnation of the silica gel with the aqueous solution of the iron(II) sulfate. The nanoparticle core consists of the iron(III) oxysulfate, and the nanoparticle surface is formed by the iron(III) hydroxysulfate

hydrate. A small amount of iron in the bulk of particles is in the divalent state, probably, due to the deficit of anion charge. The Fe^{2+} content increases with an increase in the iron concentration. The calcination of the samples containing 0.5 wt % Fe leads to the formation of iron oxide particles with a predominantly hexagonal packing of oxygen atoms. The calcination of the samples with a higher iron concentration (3FS samples) at temperatures above 500°C results in the sintering of oxide particles and the formation of ε-Fe_2O_3 oxide particles with a characteristic size of ~20 nm. The samples containing 6 wt % Fe (6FS) at calcination temperatures of 500–700°C involve metastable sulfate hydrate phase. In this case, at calcination temperatures above 500°C, the ε-Fe_2O_3 oxide particles are also formed in the 6FS samples and their number increases with an increase in the calcination temperature.

The formed particles of the iron oxide ε-Fe_2O_3 have a strongly inhomogeneous or amorphous structure. Probably, iron ions are randomly distributed over octahedral and tetrahedral positions. An analysis of the exchange interactions in the structure of the ε-Fe_2O_3 oxide in the framework of the indirect coupling model leads to the inference that this iron oxide is an eight-sublattice antiferromagnet with a strong dependence of the Néel temperature on the degree of ordering of iron ions over crystallographic positions.

Iron oxide particles are formed in the samples prepared by the incipient wetness impregnation of the aluminum oxide with the aqueous solution of the iron(II) sulfate. Most likely, this is associated with the regularity of the crystal lattice of the support. The iron oxide formed represents an ensemble of blocks with elements of the hexagonal and cubic packings of oxygen atoms. As the iron concentration increases, the fraction of blocks with the cubic packing increases and water enters into the interblock space.

ACKNOWLEDGMENTS

This study was supported by the Presidium of the Russian Academy of Sciences within the framework of the Program no. 27 "Principles of Basic Research of Nanotechnologies and Nanomaterials," Project no. 46 "Magnetically Ordered Nanoparticles in Catalytic Systems: Synthesis, Evolution, and Physicochemical Properties."

REFERENCES

1. V. Petkova and Y. Pelovski, J. Therm. Anal. Calorim. **64**, 1025; J. Therm. Anal. Calorim. **64**, 1037 (2001).
2. Y. Pelovski, V. Petkova, and S. Nikolov, Thermochim. Acta **274**, 273 (1996).
3. P. K. Gallagher, D. W. Johnson, and F. Schrey, J. Am. Ceram. Soc. **53**, 666 (1970).
4. K. S. Neto and V. K. Garg, J. Anorg. Nucl. Chem. **37**, 2287 (1975).
5. A. M. van der Kraan, Phys. Status Solidi A **18**, 215 (1973).
6. R. Zboril, M. Mashlan, D. Krausova, and P. Pikal, Hyperfine Interact. **120/121**, 497 (1999).
7. R. Zboril, M. Mashlan, and D. Krausova, in *Mössbauer Spectroscopy in Materials Science*, Ed. by M. Miglerini and D. Petridis (Kluwer, Dordrecht, The Netherlands, 1999), p. 49.
8. Y. Ikeda, M. Takano, and Y. Bando, Bull. Inst. Chem. Res., Kyoto Univ. **64**, 249 (1986).
9. D. G. Chambaere, E. de Grave, R. L. Vanleerbeerghe, and R. E. Vandenberghe, Hyperfine Interact. **20**, 249 (1984).
10. D. Chambaere, A. Govaert, J. de Sitter, and E. de Grave, Solid State Commun. **26**, 657 (1978).
11. D. Chambaere and E. de Grave, J. Magn. Magn. Mater. **42**, 263 (1984).
12. R. E. Vandenberghe, E. de Grave, C. Landuydt, and L. H. Bowen, Hyperfine Interact. **53**, 175 (1990).
13. E. de Grave, R. M. Persoons, D. G. Chambaere, R. E. Vandenberghe, and L. H. Bowen, Phys. Chem. Miner. **13**, 61 (1986).
14. E. Murad, J. Magn. Magn. Mater. **74**, 153 (1988).
15. D. R. Mabe, A. M. Khasanov, and J. G. Stevens, Hyperfine Interact. **165**, 209 (2005).
16. J. G. Stevens, A. M. Khasanov, and M. S. G. White, Hyperfine Interact. **151/152**, 283 (2003).
17. S. V. Stolyar, O. A. Bayukov, Yu. L. Gurevich, V. P. Ladygina, R. S. Iskhakov, and P. P. Pustoshilov, Neorg. Mater. **43** (6), 725 (2007) [Inorg. Mater. **43** (6), 638 (2007)].
18. S. V. Stolyar, O. A. Bayukov, Yu. L. Gurevich, R. S. Iskhakov, and V. P. Ladygina, Izv. Akad. Nauk, Ser. Fiz. **71** (9), 1310 (2007) [Bull. Russ. Acad. Sci.: Phys. **71** (9), 1286 (2007)].
19. E. Jansen, A. Kyek, W. Schafer, and U. Schwertmann, Appl. Phys. A: Solids Surf. **74** (Suppl.), S1004 (2002).
20. W. K. Wertheim and J. P. Remeika, Phys. Lett. **10**, 14 (1964).
21. I. P. Suzdalev, *Dynamic Effects in Mössbauer Spectroscopy* (Atomizdat, Moscow, 1979) [in Russian].
22. E. Tronc, C. Chaneac, and J. P. Jolivet, J. Solid State Chem. **139**, 93 (1998).
23. R. Zboril, M. Mashlan, V. Papaefthymiou, and G. Hadjipanayis, J. Radioanal. Nucl. Chem. **255**, 413 (2003).
24. K. Kelm and W. Mader, Z. Anorg. Allg. Chem. **631**, 2383 (2005).
25. I. Dezsi and J. M. D. Coey, Phys. Status Solidi A **15**, 681 (1973).
26. M. V. Eremin, Fiz. Tverd. Tela (Leningrad) **24** (2), 423 (1982) [Sov. Phys. Solid State **24** (2), 239 (1982)].
27. O. A. Bayukov and A. F. Savitskiĭ, Fiz. Tverd. Tela (St. Petersburg) **36** (7), 1923 (1994) [Phys. Solid State **36** (7), 1049 (1994)].

Translated by O. Borovik-Romanova